

---

---

# Isotope Beating Effects in the Analysis of Polymer Distributions by Fourier Transform Mass Spectrometry

Michael L. Easterling and I. Jonathan Amster

Department of Chemistry, University of Georgia, Athens, Georgia, USA

Gerard J. van Rooij and Ron M. A. Heeren

FOM Institute for Atomic and Molecular Physics, Amsterdam, The Netherlands

---

For Fourier transform mass spectrometry analysis of high mass ions, the signals from closely spaced isotope peaks undergo periodic destructive interference, producing a beat pattern in the time-domain signal. The mass spectra that are obtained by sampling transient signals for less than two beat periods exhibit an error in the relative abundances that are measured. This effect is shown to cause significant errors in the measurement of the relative abundances of the components of polymer distributions, leading to errors in the derived average molecular weights for such samples. Computer simulations show that isotope beating causes this error to increase as the duration of an acquired transient becomes short compared to the beating period. This error becomes insignificant when the transient is acquired for longer than twice the beat period. Experimental data are presented for polymers in which an oligomeric distribution of monoisotopic peaks is produced by stored waveform inverse Fourier transform ejection of all  $^{13}\text{C}$ -containing isotope peaks. The data show that the isotope beating-induced abundance errors are eliminated when there are no isotope peaks present. (J Am Soc Mass Spectrom 1999, 10, 1074–1082) © 1999 American Society for Mass Spectrometry

---

---

Mass spectrometry is becoming a widely used method for the analysis of polymer and polymer derivatives based on its reproducibility [1, 2], rapid analysis [3], and accurate mass measurement capabilities. In particular, Fourier transform ion cyclotron resonance (FT-ICR) mass spectrometry provides high mass resolution and mass accuracy which makes the technique well suited for many of the questions addressed in polymer analysis [4–18]. One of the principal strengths of FT-ICR is that a wide range of masses can be detected simultaneously. Polymer analysis naturally benefits from this capability because samples exist as a mixture of oligomers that are distributed about a defined range. The analysis of polymer endgroups, for example, benefits from the detection of several oligomer masses [15]. Although FT-ICR has advantages for the analysis of polymers, reasonable care must be taken to reduce the amount of artifactual error introduced at each step of the experiment. For example, mass discrimination effects in trapping either externally or internally generated ions can skew the observed oligomer distribution. Optimization of trapping conditions is required to reduce time-of-flight or

energy filter effects [19–21]. Quenching of excess kinetic energy after the trapping event may also be required to prevent the high mass end of the distribution from escaping the cell, especially if trap potentials are decreased prior to detection. Excitation using an rf waveform with a relatively flat power frequency spectrum such as a stored waveform inverse Fourier transform (SWIFT) [22] pulse reduces artifacts resulting from the uneven power distribution found in the commonly used linear rf chirp. Additionally, ion densities during excitation should be optimized to reduce amplitude errors resulting from space-charge effects [23].

This paper presents another source of error in measuring the proper relative abundances of oligomers in a polymer distribution that is inherent to the FT-ICR detection method. The FT-ICR technique is based on the measurement of the image charge induced on the detection electrodes by the coherent cyclotron motion of ions trapped in the analyzer cell. The signal at the detector is simply the sum of the instantaneous phases and amplitudes of the individual oscillators. Depending on the relative phase of the oscillators, this may lead to constructive or to destructive interference. As a result, the time domain signal is a complex waveform containing a manifold of frequency components corresponding to the different oscillators. The Fourier analysis method transforms this complex waveform into a frequency

---

Address reprint requests to I. Jonathan Amster, Department of Chemistry, University of Georgia, Athens, GA 30602-2556. E-mail: Amster@sunchem.chem.uga.edu

domain function that describes the individual frequencies and their magnitudes. This information is used to determine the mass-to-charge values and the abundances describing the ion population.

Modulation effects in the transient produced by interference are often observed with electrospray ionization (ESI) FT-ICR. The small frequency separation between isotopes for highly charged, high mass ions results in a phenomenon known as isotope “beating” [24]. Some degree of modulation is usually observed in the time domain transients of FT-ICR spectra of most materials, regardless of the sample or ionization conditions. However, the modulation periods for heavy ions produced by ESI can approach 10–20 s in length, even for highly charged ions. High mass ions, with large numbers of closely spaced isotope peaks, produce a transient signal in which short bursts of data are separated by long periods (dictated by the modulation frequency) of little or no observable signal above the broadband spectral noise. Although the mass information provided by these transients is not compromised by modulation of the time domain data, longer acquisitions are required to achieve high resolution spectra that can be used to determine the charge state from isotope peak separation [24]. The beating phenomenon is illustrated by the data of Figure 1, which shows the time-domain signals obtained for the ESI FT-ICR of three proteins of various charge states and molecular weights.

The theoretical description pertaining to modulation effects between closely spaced oscillators is fairly simple, and can be derived from basic trigonometric identities [24]. In the case of isotope beating, the modulation frequencies are determined by the frequency separation between adjacent isotope peaks. Although the number of isotope peaks for heavy ions can be quite considerable, the variation in the frequency difference between any pair of adjacent peaks is small, allowing the overall “beat” frequency to be estimated by the characteristic frequency spacing for a given charge state. This characteristic beat frequency (in Hz) is closely approximated by eq 1, where  $z$  is the integer number of elementary charges on the ion,  $m$  is mass in u, and  $B$  is the magnetic field strength in tesla. For example, an ion of mass 10,000 with 10 charges at a magnetic field strength of 7 tesla, exhibits a major beat of 11 Hz ( $\tau = 90$  ms):

$$\Delta f \cong \frac{zB}{2\pi m^2} \times 10^8 \quad (1)$$

Previous work concerning isotopic modulation effects has been concerned with the effect on mass resolution [24], but has not addressed the impact on the magnitude of spectral peaks. Here, we address the effect of isotope beating on the measured relative abundances of a distribution of ions. The key question for polymer analysis concerns the manner in which the beating phenomenon alters the individual abundances

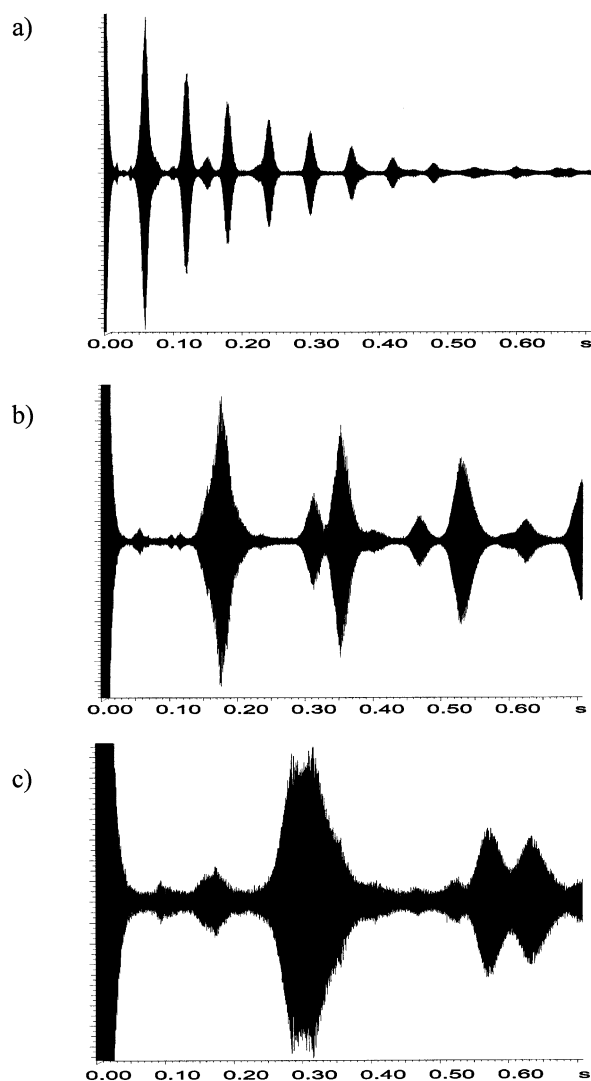


**Figure 1.** Time domain transients for (a) the 5+ charge state of bovine insulin ( $M_w = 5729$ ), (b) the 8+ charge state of cytochrome *c* ( $M_w = 12,360$ ), and (c) the 10+ charge state of myoglobin ( $M_w = 17,554$ ), collected at a field strength of 7 tesla, showing the effect of isotopic beating which creates periodic regions of diminished signal with a beat frequency (period) that is calculated by using eq 1 to be (a) 17 Hz (60 ms), (b) 5.8 Hz (170 ms), and (c) 3.6 Hz (280 ms). Additional beats are observed from ions of other charge states that are present at low abundance.

of mass peaks and how these changes affect the quantitative characterization of polymer distributions. Several well documented effects are known to affect peak magnitudes in FT-ICR including space charge [23], rf excitation nonlinearities [25], and dynamic coulombic interactions of ion clouds with different frequencies during detection [26]. All of these effects are a result of physical conditions during the excitation/detection process. Intermodulation, however, is independent of these parameters, existing as a result of the interference between waves traveling through a common medium.

By modeling the behavior of transients, we can determine the effect of multiple modulation frequencies

on the relative abundance distributions of mass spectra containing many peaks independently of other significant physical effects. Although the data and models presented here are primarily involved with the mass information found in polymer distributions, it is reasonable that samples with multiple, closely spaced masses such as petrochemicals, combinatorial libraries, and natural products would exhibit similar effects.

## Experimental

### Numerical Simulations

To separate the effects of signal interactions from other physical phenomena, evaluations were first carried out using simulated transients generated by computation. Transient data was produced with a custom program running on a 180 MHz MIPS R5000 based Silicon Graphics workstation (Silicon Graphics, Mountain View, CA). The source code was written in the C programming language and compiled and optimized by the MIPS PRO compiler and associated math libraries and is available upon request. Simulated transients were produced by coding an array of individual mass and abundance values for a polymeric distribution, or by providing the program with key distribution parameters such as mean, standard deviation, and repeat mass to allow automatic generation of mass and abundance values. The expression used to determine the amplitude of the set of oscillators for each timepoint is given by eq 2, where  $i$  is an index for each oligomer unit,  $j$  is an index for each isotope peak of a given oligomer unit,  $B$  and  $C$  are the abundance values for each oligomer unit and its isotope distribution, respectively,  $n$  is the time index,  $f$  is the unperturbed cyclotron frequency for each mass, and  $t$  is the time computed as the product of an integer index and the reciprocal sampling rate. Isotope abundances,  $C_j$ , were calculated for an oligomer of the average molecular weight using the IsoPro [27] program. The oligomer abundances,  $B_i$ , were estimated by a gaussian function with the mean equal to the center mass and  $\sigma = 300$  Da, to approximate a polymer distribution of near unit polydispersity.

$$A(n) = \sum_i^{\text{all oligomers}} \sum_j^{\text{all isotopes}} B_i C_j \sin(2\pi f_{i,j} n \Delta t) \quad (2)$$

At each time point, defined by an incremental counter multiplied by the time step size, an instantaneous amplitude is calculated by summing together the amplitudes for each isotope and for all oligomers. Broadband noise was not included in the simulation, and isotopic abundance ratios for each polymer repeat unit were treated the same as that of the central peak, as the abundances do not vary greatly for the major peaks in distributions with low polydispersity indices. Data manipulation and evaluation including fast Fourier transform (FFT) and mass calibration was performed

using the XMGR data analysis program compiled for the SGI workstation. This program provided a utility for handling the large data sets produced by the simulations, which approached 30 MB in length. All simulated distributions were windowed by the Hanning function prior to performing the FFT. Additionally, zero filling data sets eliminated significant errors in relative abundance that are often observed for spectra that had not been zero filled. Data sets shorter than 256 K were zero filled to 256 K, while 256 K transients were zero filled to 512 K. No assumptions were made with regards to actual experimental conditions with respect to experimental phase lag resulting from chirp excitation, the delay between excitation and detection or ion cloud evolution effects such as dephasing [28, 29], signal locking [30–33], or dampening [34].

### Instrumental

The matrix-assisted laser desorption/ionization (MALDI) FT-ICR experiments are performed on two different instruments. The first is an internal 4.7 tesla system designed and constructed at the University of Georgia, and has been described previously [16]. Briefly, a multisample MALDI target is positioned about 1 cm behind an open, cylindrical cell along the magnetic axis. The 355 nm line of a pulsed YAG laser is pulsed for the MALDI event, followed by gated trapping and collisional cooling of the trapped ions. Prior to detection, trapping potentials are lowered to 250–750 mV and capacitive coupling is restored by an isolation circuit that prevents time-lag effects on gated trapping resulting from the coupling circuit [19].

A second instrument was used for the isolation experiments that were performed at the FOM institute on a modified APEX 7.0e FTICR-MS (Bruker-Spectrospin, Fallanden, Switzerland) equipped with a 7-tesla magnet and an in-house designed external ion source. Instrumental and experimental details can be found in previously published papers [6, 15]. The timing sequences used for the external ion source MALDI experiments and their effect on the Fourier transform mass spectrometry (FTMS) data have been described previously [35]. In short, a gated channel in the electrostatic potential well of the ICR trap is created, allowing the ions to enter the cell. The rear trapping electrode remains at typically 3.5 V. The channel in the front trapping potential is closed by applying a 2.5 V potential to all elements of the front trap electrode after a variable period of time. The finite accumulation time during an experiment will cause a pulsed external ion source FTMS to exhibit flight time discrimination [35]. The asymmetry in the trapping field is introduced because it gives an optimal signal to noise ratio in these experiments.

Ion selection for the polymer samples studied with the 7 tesla instrument has been carried out using a home-built arbitrary waveform generator (AWG). It has 192 MB of random access memory (RAM) and a 40

MHz, 12 bit digital-to-analog converter available to store and generate tailored frequency pulses with a maximum bandwidth of 20 MHz. The experiments described in this article use an adapted SWIFT algorithm [22, 36, 37] to calculate the distribution of excitation power over the duration of the excitation pulse. The calculated waveform is downloaded from the SGI workstation into the AWG memory. A small relay switching circuit connects either the output of the programmable frequency synthesiser or the AWG output to the transmitter. A TTL trigger pulse toggles this switching circuit. A second TTL trigger pulse is generated 3 ms later, when the relays have settled. This pulse triggers the AWG to output the loaded excitation waveform. The X-windows software generating and controlling the AWG was developed at the FOM institute. Details of this experimental setup will be described elsewhere.

## Results and Discussion

The relatively high ionization efficiency of several classes of industrial homopolymers make them quite useful for diagnostics and calibration, especially in MALDI-FTMS [16, 18]. Characteristic symmetrical distributions allow experimental optimization of the conditions needed to analyze a wide mass range and provide feedback on the effectiveness of ion manipulation events such as ion trapping, excitation, collisional dissociation, and axialization for target mass ranges. Both polar and nonpolar polymers are routinely used for these purposes in the 4.7 tesla internal and 7.0 tesla external MALDI FT-ICR instruments. It was discovered, however, that changes in the data set size used for the FFT of acquired spectra would result in changes in the observed polymer weight distribution. An example of this effect is shown for a PEG 2000 sample in Figure 2. The top panel shows the mass spectrum resulting from a 128 K data set acquired over 262 ms in the 4.7 tesla instrument. The polymer distribution resembles the expected gaussian profile for this sample, evenly distributed about the expected average mass, represented by the line around  $m/z$  2075. The middle panel shows the mass spectrum resulting from transforming the first 64 K of the same data set. Although a regular distribution is generally retained, some flattening and skewing is visible about the expected center mass. For the bottom panel, in which the mass spectrum is truncated half again to 32 K, a large variation about the expected center mass is observed with a complete loss of symmetry. This mass distribution has clearly been skewed to favor lower mass ions.

The effects of signal interferences on the spectral amplitude distribution cannot be completely determined in situ. Although the frequency dependent power differences resulting from chirp excitation might be eliminated by SWIFT excitation [22], and space

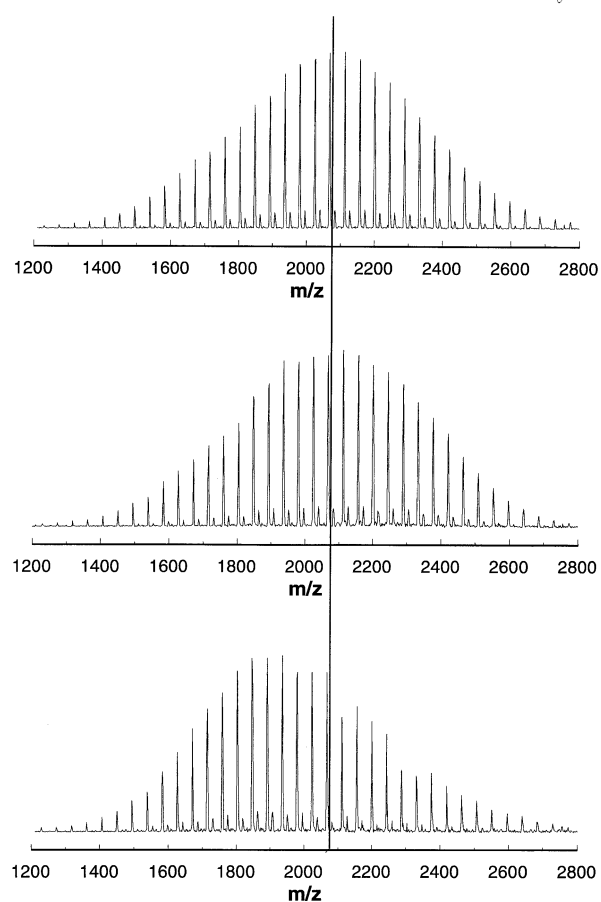


**Figure 2.** Experimentally obtained mass spectra for a MALDI generated PEG 2000 distribution on the 4.7 tesla instrument resulting from the Fourier transform of (a) the full 128 K data set (232 ms transient), (b) the first 64 K of the data set, and (c) the first 32 K of the data set. The vertical line that crosses the three spectra corresponds to the number average molecular weight ( $M_n$ ) of the polymer, 2075 Da.

charge amplitude effects reduced by using a relatively low ion population, several other uncontrollable or unknown processes might effect the phase or amplitude of the rotating ion packets over time [29, 30, 38, 39]. To avoid these problems, numerically calculated time domain transients were used to investigate the effect of interference between closely spaced isotopic frequencies on the measured polymer distributions.

Time domain data for a mass-to-charge distribution closely matching that of the experimentally observed sample of Figure 2 were generated using a computer program. One transient was generated by summing sine waves with frequencies corresponding to each of the peaks (including isotopes) for a polymer with an oligomer distribution similar to that of Figure 2a. It was observed to have well-defined amplitude oscillations regularly spaced in time. A second transient was generated by computer assuming ions of monoisotopic mass only, occurring at the polymer repeat interval. This transient was found to exhibit a much smoother time domain profile due to the lack of closely spaced

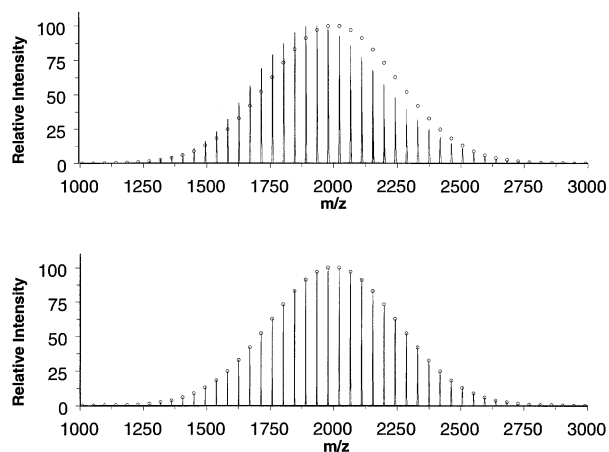


**Figure 3.** (Top) Fourier transform of the first 32 K data points of a computer-generated transient for an isotope-containing distribution and (bottom) a monoisotopic distribution. The open circles correspond to the abundance values of the distribution used to generate the transient. The isotope-containing data set (top) is observed to produce a skewed distribution, whereas the monoisotopic data (bottom) closely matches the expected distribution.

frequency components that produce low frequency modulation.

Transformed data using Hanning apodization for the leading 32 K points of the 256 K computer-generated data is shown at the top of Figure 3. For comparison with expected values, theoretical peak magnitudes used to generate the waveform are shown as open circles with the highest abundance value normalized with the transformed data set. Although the distribution is somewhat symmetric, skewing in favor of the lower half of the distribution is observed for the short transient from the isotope-containing model. These errors resemble those found for an experimentally obtained transient of similar length.

The lower half of Figure 3 shows the transformation of the corresponding computer-generated monoisotopic time domain data of equal length. The masses calculated in this case lie within the peak heights of the model distribution and shifts in the centroid distribution are not apparent. This qualitative correlation between these results and the experimental data indicates that the centroid shifts observed for polymer distributions are principally attributable to the interference effects of closely spaced isotope frequencies. It should be stressed that although abundances are affected, the measured frequencies are not altered by this effect, as dictated by the superposition theorem. Figure 4 shows that the full 256 K data set transforms into mass distributions that closely match expected values for the isotope-containing (top of figure) and monoisotopic (bottom of figure) cases.

Computer generated transients corresponding to the expected distribution of singly charged polymethyl methacrylate (PMMA) ions ( $M_r$  1000) for the monoisotopic and isotope-containing cases were calculated for a

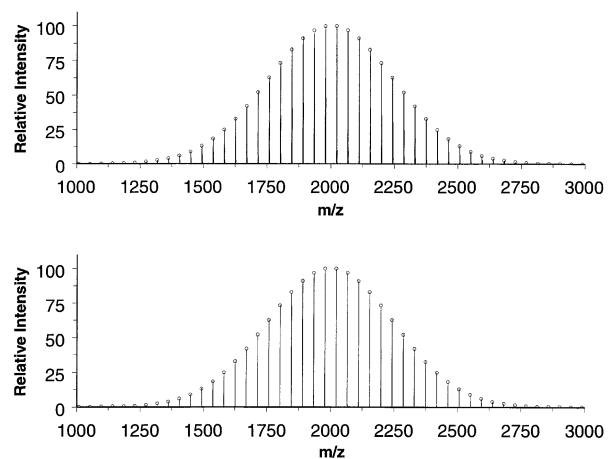


**Figure 4.** Fourier transform of 256 K data points of the computer-generated transients used for Figure 3, with isotope-containing (top) and monoisotopic distributions (bottom). Both data sets are found to closely match the expected distribution (open circles).

7 tesla magnetic field strength with 128 K acquired data points (131 ms transient for 1 MHz sampling rate), and are shown in Figure 5. In order to determine if the amplitude associated with each mass in the isotope-containing polymer distribution is variant over the life of the transient, the data sets were split into 32 blocks containing 4 K of data per block, and selected blocks were transformed into mass spectra. The equal length blocks provide peaks of similar spectral linewidth so that peak height, rather than area, can be used as a consistent measure of relative ion abundance. As in the previous data, dynamic processes that naturally occur during the lifetime of ion detection such as broadening mechanisms [34], and signal locking [28, 31, 33, 40] were not considered.

Figure 6 shows the results of Fourier transformation of selected blocks of the isotope-containing computer-generated transient corresponding to a PMMA 1000 distribution. Each section of transient is observed to produce a set of significantly different abundances for the given range of masses, although the distribution shape is fairly well defined for all of the data blocks. Computer-generated mass spectra from monoisotopic oligomer distributions, shown in Figure 7, indicate no observable oscillation in the magnitudes of the polymer masses, but rather exhibit identical abundances for each transformed block. This demonstrates that the presence of isotope beating leads to an “instantaneous” error in the abundance distribution.

Such effects are seen in experimentally obtained mass spectra of polymers. Figure 8 shows mass data transformed from 1 K segments of a transient as a function of time for experimentally obtained transients from a PMMA 1000 distribution acquired at 7 tesla. Figure 8a was obtained from an isotope-containing distribution. Figure 8b shows the data obtained when all but one of the isotopes for each oligomer was removed by resonance ejection using an arbitrary wave-

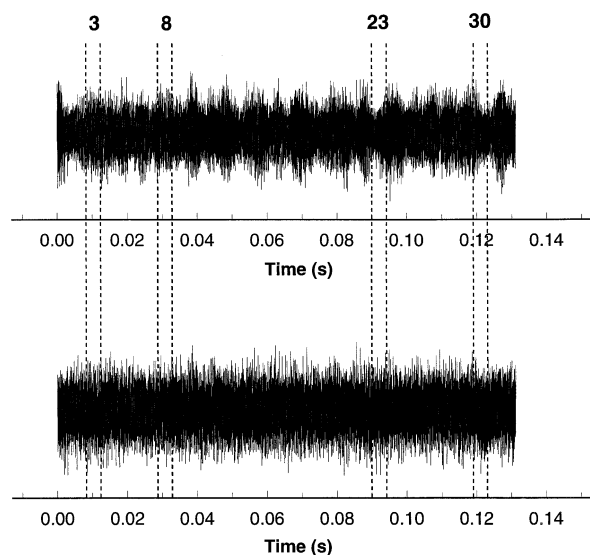


**Figure 5.** Computer-generated time-domain transients corresponding to a PMMA 1000 distribution, calculated for a 7 tesla magnetic field strength for both (top) isotope-containing and (bottom) monoisotopic masses. The dotted line indicate boundaries for sets of 4 K data points extracted at various times to compare the instantaneous distribution of abundances.

form generator. The plot in Figure 8a clearly depicts the staggered nature of the isotope beats, which indicates that a sampling time of less than 0.02 s would not completely sample the first beat of the 1400 Da oligomer. A similar plot for the monoisotopic case, shown in Figure 8b, indicates an absence of beating, which is consistent with the invariance in amplitude over time observed in Figure 7.

To prove that the oscillations in the measured relative abundances of the components of a polymer distribution can be fully attributed to isotope-induced beat frequencies, a series of experiments were performed on a PMMA sample with an average molecular weight of 1140 Da using the 7 tesla instrument. These experiments were carried out at a gated trapping time of 1000  $\mu$ s, and no time-of-flight correction [35] was applied. Variation in the abundances in the course of the transient are again visualized by dividing the transient into 32 blocks of 4 K size and transforming these blocks into mass spectra. The mass spectra of selected blocks as well as the spectrum obtained from the entire transient are shown in Figure 9. It is seen that the variations in the measured distributions are similar to those observed in the numerically simulated data set in Figure 6. However, the signal-to-noise ratio in the experimentally obtained mass spectra is observed to decrease towards the end of the transient, whereas in the case of the simulated transient this ratio remains roughly constant. This results from signal dampening, which was not included in the simulations. Isotope-depleted experimental data were obtained by using the arbitrary waveform generator to isolate the monoisotopic peaks. All other peaks were eliminated by resonant ejection from

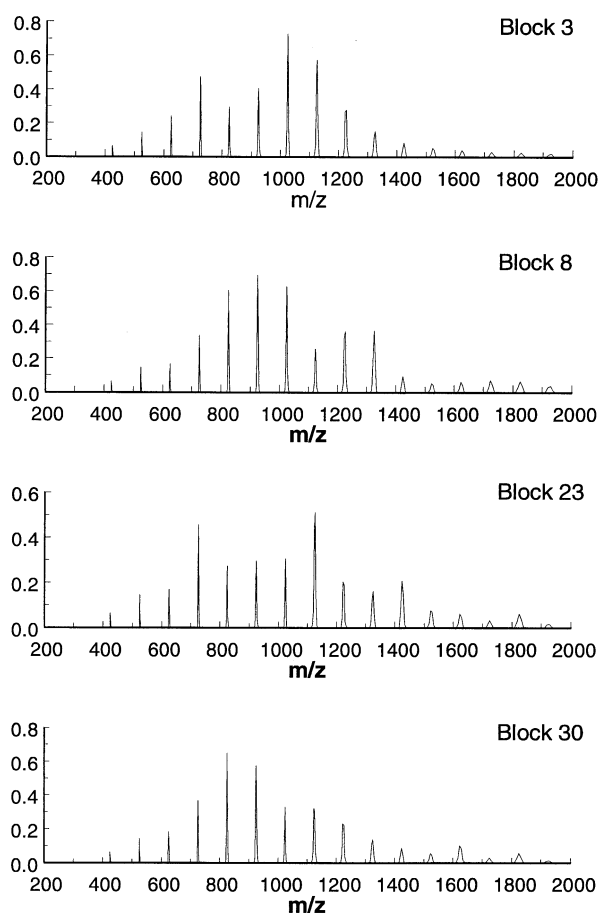


**Figure 6.** Transformed spectra for the data sets extracted from a computer-generated isotope-containing time domain transient, indicating differences in the instantaneous abundances of the observed masses for the isotope containing distribution.

the analyzer cell. In Figure 10, mass spectra of selected blocks of 4 K size are presented for the isotope-depleted distributions. As observed in the simulations, the shape of the apparent mass distribution remains unchanged over the entire transient.

Comparison of the mass spectra of the entire transients in Figures 9 and 10 reveals that the apparent molecular weight distribution changes significantly by removal of the isotopes from the analyzer cell. The apparent number average molecular weight ( $M_n$ ) increases from 1044 to 1104, and the weight average value ( $M_w$ ) shifts from 1084 to 1151 when the isotopes are ejected. For comparison, the manufacturer's values for  $M_n$  and  $M_w$  are 1073 and 1192 Da. Closer inspection of the distribution in Figure 10 suggests that the abundance of the  $m/z$  925 ion is severely underestimated. Imperfections in the isolation waveform might be responsible for this effect, as they can affect the distribution through off-resonance excitation. However, it is unlikely that this would affect only one component in the distribution, as all notches in the frequency spectrum are symmetrically centered around the monoiso-

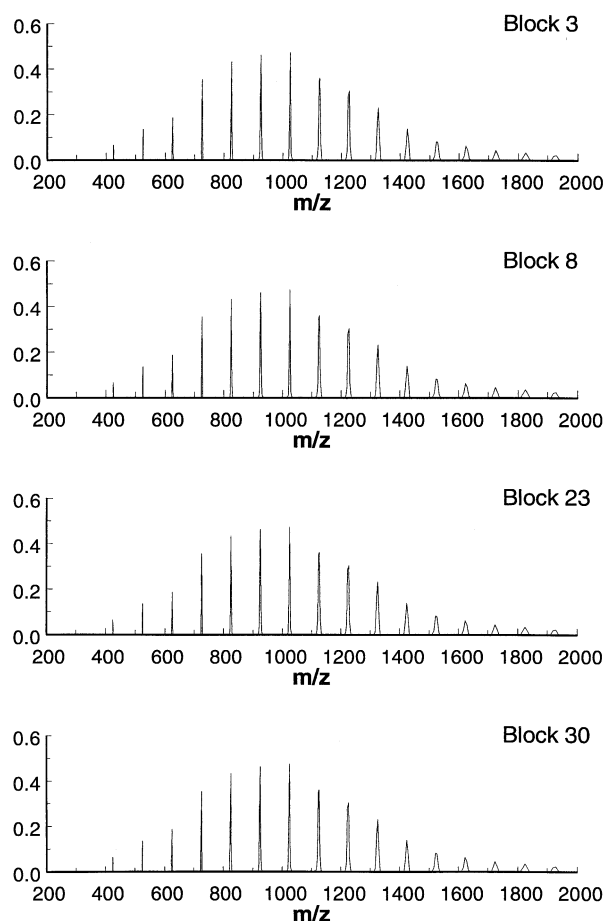


**Figure 7.** Transformed spectra for the data sets extracted from a computer generated monoisotopic time domain transient indicating no significant amplitude variations between data blocks.

topic peaks and are of equal abundance. Furthermore, previous isolation experiments on various samples have never revealed such effects. Other experimental artifacts could also produce this result, such as shot-to-shot variations in the ion cloud evolution. If we assume that the distributions in Figure 9 do represent the actual ion population inside the analyzer cell, then it is striking to see the similarity between the spectra of block 23 and 30 in Figure 9 (containing all isotopes) and the spectra in Figure 10 (containing only the monoisotopic oligomer ions.) The convergence of these two series of spectra is most likely a result of ion cloud evolution that favors the most populated mass channels. This effect has recently been attributed to coulombic shearing forces that preferentially dephase sparser ion clouds causing them to dampen before the denser ion clouds [41]. Additionally, the weak presence of only a few mass channels virtually eliminates the beating effect, as observed as smoothness in the contour plots. As a result of these effects, the “instantaneous” mass distributions for both the isotope-containing and depleted transients are observed to converge over the life of the transient.

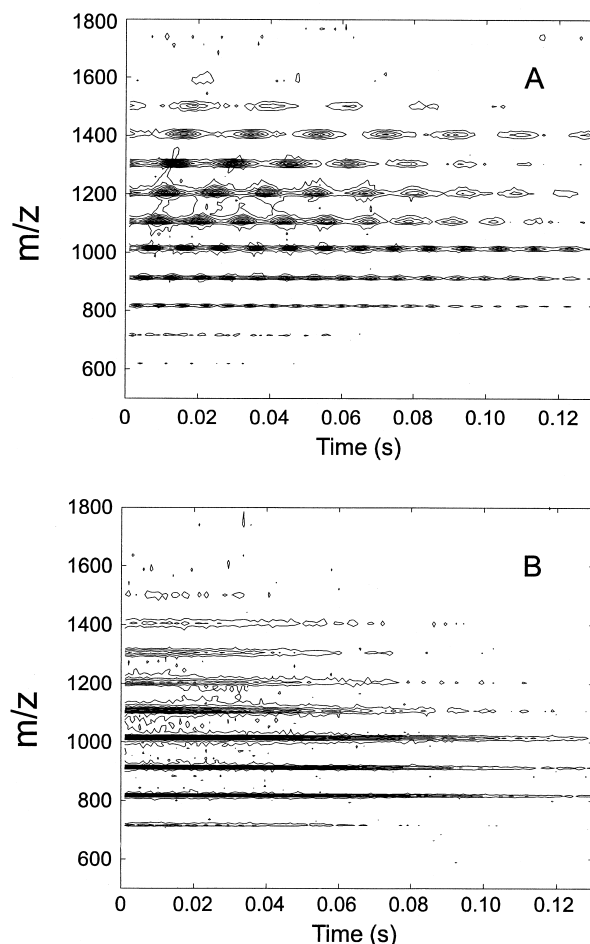


**Figure 8.** Contour plots of experimentally obtained data from a PMMA 1000 distribution, acquired at 7 tesla. Contours of signal amplitude are plotted as a function of both time and mass-to-charge ratio. Densely spaced contour lines indicate regions of high signal amplitude. (a) An amplitude modulation is observed for each component of the mass distribution as a function of time for the isotope-containing ions. (b) The monoisotopic distribution exhibits a fairly uniform mass abundance for the duration of the transient.

The similarity of the final mass spectra from the final blocks of data supports our contention that the initial oligomer distributions were the same.

Examining small pieces of the time domain transients would be expected to yield mass spectra with varying abundances if beating effects created a discriminating sampling condition. In this case, a nonuniform number of maxima, or beats, are sampled for each frequency in the spectrum. Of greater importance to the analytical study of polymers is how the beating phenomenon affects abundance information for larger data sets, those in which the sample size provides Fourier-limited resolving power for baseline isotope separation. Experimental observation from Figure 2 indicated that centroid shifts are less significant for larger data set sizes. Table 1 shows that the theoretically produced data sets exhibit this behavior. The calculated weight

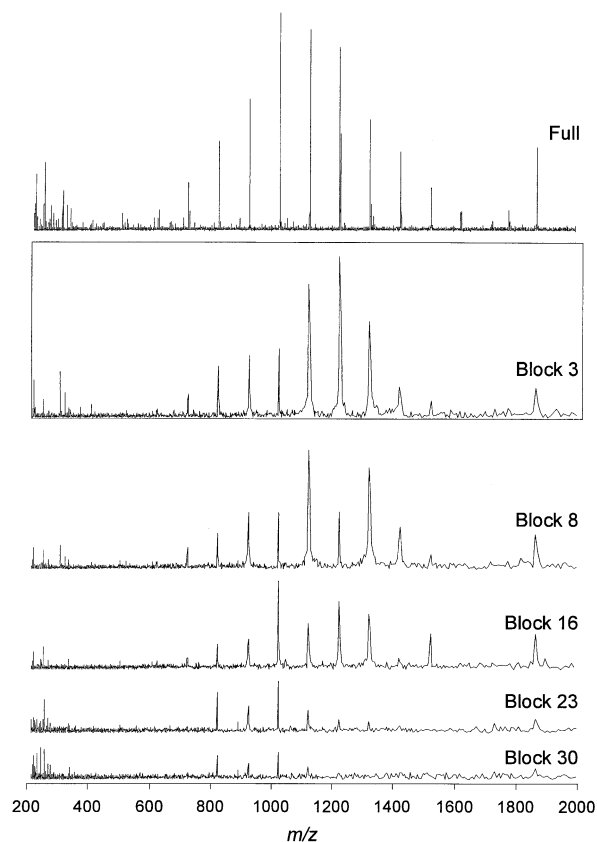


**Figure 9.** Experimentally obtained mass spectra of a PMMA 1000 distribution for the full transient and selected 4 K blocks. As with the simulated data, random oscillations of mass abundances are observed for each block.

average for the isotope-containing PEG 2000 theoretical distribution (expected  $M_w = 2032.13$  Da) is seen to drop from a 5% error for the 32 K data set, to an error of about 1% for the 128 K transient. The 32 K transient would represent an acquisition time of about 66 ms sampling for a bandwidth of 250 kHz, slightly longer than the isotopic beat period for the central mass (58 ms). The 8 ms sampling time provided by the 4 K transient only represents about 15% of the beat period, resulting in large errors observed for transients of that length. A significant decrease in error is observed for the 64 K transient, for which 131 ms utilizes the magnitude information provided by two isotopic beats. From these data, it can be inferred that sampling for a period equal to the duration of two isotope-induced beats should be a minimum requirement to obtain a proper quantitative description of a polymer distribution. Slightly greater precision is obtained by further averaging of the instantaneous differences for an isotope containing distribution, as mentioned above for the 128 K transient which samples more than four isotope beats of the center mass.

As determined earlier, the errors for the monoisotopic distribution are not observed to significantly fluctuate for changes in data set size. These results quanti-

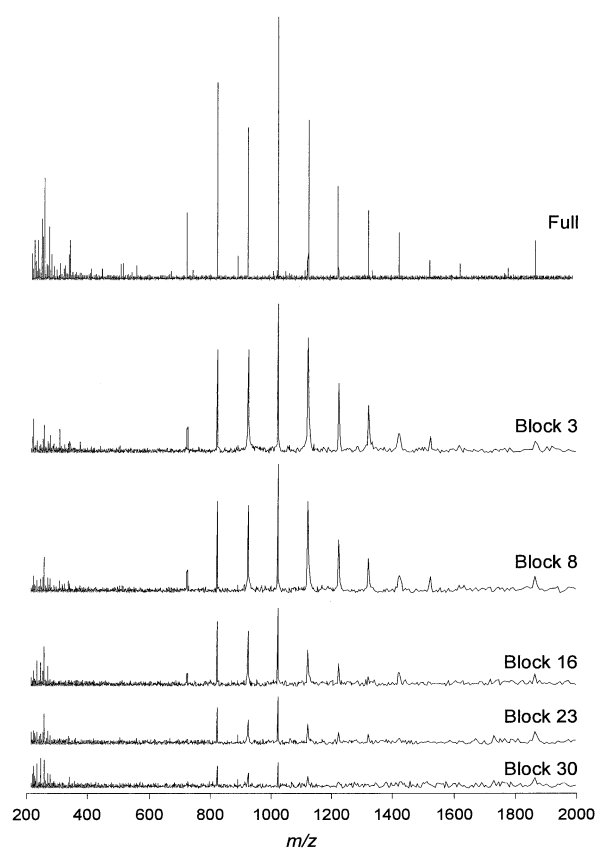


**Figure 10.** Experimentally obtained mass spectra of a PMMA 1000 distribution containing only monoisotopic peaks for the full transient and selected 4 K blocks. Abundances are not observed to vary significantly as in the isotope containing spectra shown in Figure 9.

tatively support the earlier finding that longer transients tend to provide better  $M_w$  values for polymers. The longer sampling times inherently provide larger windows in which the disparity in the number of amplitude maxima for represented frequencies becomes smaller.

## Conclusions

To accurately measure relative abundances for large distributions of ions that contain closely spaced masses, transient duration must be considered to avoid the errors produced by isotopic beating in the time domain transient. The appropriate duration will depend on the magnetic field strength and mass and abundance distributions. Providing an analytical expression for the required sampling time for polymers is somewhat complex because the beat period is significantly different for the two ends of the distribution. To be conservative, the minimum sample time should be two beat periods calculated for the frequency difference between isotope peaks at the high mass end of the oligomer distribution. Verification that the transient is sufficiently long would require performing an FFT on multiple truncations of

**Table 1.** Average molecular weights calculated from theoretical transients of different length for a PEG 2000 distribution with  $M_w = 2032.13$  Da. Significant error is observed for the small data set of the isotope-containing transient. The error is sharply reduced as more data is sampled. In contrast, the data generated for monoisotopic distributions provides an accurate average molecular weight even for small data sets

		With isotopes	Without isotopes
32 K	$M_w$	1933.49 (−98.64)	2031.26 (−0.87)
64 K	$M_w$	2024.93 (−7.20)	2030.00 (−2.13)
128 K	$M_w$	2029.45 (−2.68)	2031.41 (−0.72)

the data set. As described earlier, the distributions will converge to a given central value as the data set size is increased. Convergence of the centroid indicates that sufficient sampling has been performed. It should be noted however, that the data found towards the end of the experimentally obtained transient is usually weighted much lower than that found at the beginning due to collision-induced signal dampening [34]. Also, other temporally evolving effects such as nonuniform decay and magnitude dependent ion cloud destabilization [26] should be considered when seeking longer transients. These considerations aside, accurate relative abundances can be obtained by sampling sufficient data points.

## Acknowledgments

Financial support by the National Science Foundation (CHE-9412334) is gratefully acknowledged. Financial support for the FOM instrument was provided by the IAS instrument development program for advanced mass spectrometry, the Nederlandse organisatie voor Wetenschappelijk Onderzoek (NWO, Dutch organization for scientific research), and the foundation for Fundamenteel Onderzoek der Materie (FOM). This research was performed as part of the FOM programme nr. 28 "Biomacromoleculair Mass Spectrometry."

## References

- Haefliger, O. P.; Zenobi, R. *Rev. Sci. Instrum.* **1998**, *69*, 1828–1832.
- Axelsson, J.; Hoberg, A. M.; Waterson, C.; Myatt, P.; Shield, G. L.; Varney, J.; Haddleton, D. M.; Derrick, P. J. *Rapid Commun. Mass Spectrom.* **1997**, *11*, 209–213.
- Qian, K. N.; Killinger, W. E.; Casey, M.; Nicol, G. R. *Anal. Chem.* **1996**, *68*, 1019–1027.
- Brenna, J. T.; Creasy, W. R. *Appl. Spectrosc.* **1991**, *45*, 80–91.
- vanderHage, E. R. E.; Duursma, M. C.; Heeren, R. M. A.; Boon, J. J.; Nielsen, M. W. F.; Weber, A. J. M.; deKoster, C. G.; deVries, N. K. *Macromolecules* **1997**, *30*, 4302–4309.
- Heeren, R. M. A.; Dekoster, C. G.; Boon, J. J. *Anal. Chem.* **1995**, *67*, 3965–3970.
- Limbach, P. A.; Kim, H. S.; Hill, N. C.; Marshall, A. G. *Anal. Chim. Acta* **1993**, *277*, 31–39.
- Castoro, J. A.; Koster, C.; Wilkins, C. L. *Anal. Chem.* **1993**, *65*, 784–788.
- Oconnor, P. B.; McLafferty, F. W. *J. Am. Chem. Soc.* **1995**, *117*, 12826–12831.
- Campana, J. E.; Sheng, L. S.; Shew, S. L.; Winger, B. E. *Trac-Trends Anal. Chem.* **1994**, *13*, 239–247.
- Liang, Z. M.; Marshall, A. G.; Westmoreland, D. G. *Anal. Chem.* **1991**, *63*, 815–818.
- Brenna, J. T.; Creasy, W. R.; Zimmerman, J. *Adv. Chem. Ser.* **1993**, 129–154.
- Dekoster, C. G.; Duursma, M. C.; Vanrooij, G. J.; Heeren, R. M. A.; Boon, J. J. *Rapid Commun. Mass Spectrom.* **1995**, *9*, 957–962.
- vanRooij, G. J.; Duursma, M. C.; Heeren, R. M. A.; Boon, J. J.; deKoster, C. G. *J. Am. Soc. Mass Spectrom.* **1996**, *7*, 449–457.
- Heeren, R. M. A.; Boon, J. J. *Int. J. Mass Spectrom. Ion Processes* **1996**, *158*, 391–403.
- Easterling, M. L.; Mize, T. H.; Amster, I. J. *Int. J. Mass Spectrom. Ion Processes* **1997**, *169*, 387–400.
- Pastor, S. J.; Wood, S. H.; Wilkins, C. L. *J. Mass Spectrom.* **1998**, *33*, 473–479.
- Pastor, S. J.; Wilkins, C. L. *Int. J. Mass Spectrom. Ion Processes* **1998**, *175*, 81–92.
- Easterling, M. L.; Pitsenberger, C. C.; Amster, I. J. *J. Am. Soc. Mass Spectrom.* **1997**, *8*, 195–198.
- Guan, S. H.; Pasatolic, L.; Marshall, A. G.; Xiang, X. Z. *Int. J. Mass Spectrom. Ion Processes* **1994**, *139*, 75–86.
- Koster, C.; Castoro, J. A.; Wilkins, C. L. *J. Am. Chem. Soc.* **1992**, *114*, 7572–7574.
- Marshall, A. G.; Wang, T. C. L.; Ricca, T. L. *J. Am. Chem. Soc.* **1985**, *107*, 7893–7897.
- Uechi, G. T.; Dunbar, R. C. *J. Am. Soc. Mass Spectrom.* **1992**, *3*, 734–741.
- Hofstadler, S. A.; Bruce, J. E.; Rockwood, A. L.; Anderson, G. A.; Winger, B. E.; Smith, R. D. *Int. J. Mass Spectrom. Ion Processes* **1994**, *132*, 109–127.
- Marshall, A. G.; Roe, D. C. *J. Chem. Phys.* **1980**, *73*, 1581–1590.
- Bresson, J. A.; Anderson, G. A.; Bruce, J. E.; Smith, R. D. *J. Am. Soc. Mass Spectrom.* **1998**, *9*, 799–804.
- IsoPro 3.0, MS/MS Software, <http://members.aol.com/mmssoft>
- Naito, Y.; Inoue, M. *Int. J. Mass Spectrom. Ion Processes* **1996**, *158*, 85–96.
- Nikolaev, E. N.; Miluchihin, N. V.; Inoue, M. *Int. J. Mass Spectrom. Ion Processes* **1995**, *148*, 145–157.
- Peurrung, A. J.; Kouzes, R. T. *Int. J. Mass Spectrom. Ion Processes* **1995**, *145*, 139–153.
- Mitchell, D. W.; Smith, R. D. *Phys. Rev. E* **1995**, *52*, 4366–4386.
- Stults, J. T. *Anal. Chem.* **1997**, *69*, 1815–1819.
- Huang, J. Y.; Tiedemann, P. W.; Land, D. P.; McIver, R. T.; Hemminger, J. C. *Int. J. Mass Spectrom. Ion Processes* **1994**, *134*, 11–21.
- Marshall, A. G.; Comisarow, M. B.; Parisod, G. J. *Chem. Phys.* **1979**, *71*, 4434–4444.
- Oconnor, P. B.; Duursma, M. C.; vanRooij, G. J.; Heeren, R. M. A.; Boon, J. J. *Anal. Chem.* **1997**, *69*, 2751–2755.
- Guan, S. H.; Marshall, A. G. *Int. J. Mass Spectrom. Ion Processes* **1996**, *158*, 5–37.
- Guan, S. H.; Marshall, A. G. *Anal. Chem.* **1993**, *65*, 1288–1294.
- Naito, Y.; Inoue, M. *Rapid Commun. Mass Spectrom.* **1997**, *11*, 578–586.
- Mitchell, D. W.; Smith, R. D. *Int. J. Mass Spectrom. Ion Processes* **1997**, *165*, 271–297.
- Mitchell, D. W.; Smith, R. D. *J. Mass Spectrom.* **1996**, *31*, 771–790.
- Bresson, J. A.; Anderson, G. A.; Bruce, J. E.; Smith, R. D. *J. Am. Soc. Mass Spectrom.* **1998**, *9*, 799.